Vibrational and electronic absorption study of bistable and stable $F_H(OH^-)$ centers in alkali halides

Volkmar Dierolf and Fritz Luty
Physics Department, University of Utah, Salt Lake City, Utah 84112
(Received 1 April 1996)

The closest possible F center-OH^- defect pairs, located on $\langle 200\rangle$ next-nearest-neighbor anion sites separated by a host cation, have been studied in terms of their electronic (EA) and stretching-mode vibrational absorption (VA) in various hosts. These pairs can exist in KBr, RbBr, and RbI at $T \lesssim 10$ K in two different bistable configurations B and R, characterized by partially overlapping electronic absorptions (blue and red shifted from the F band), and by spectrally well separated sharp VA lines. Irradiation into the B and R electronic bands achieves at 4 K reversible $B \rightleftarrows R$ conversions, which we determined to occur in both directions with high (0.2–0.6) quantum efficiency. Fourier-transform infrared measurements parallel to these EA conversions established the proper assignment of the two VA lines to the B and R configurations (and yielded their oscillator strength ratio). Guided by recent electron nuclear double resonance results in KBr: OH^-, we attribute bistability and the observed EA and VA behavior to large linear off-center displacements of the cation between F and OH^- along the pair axis, which is strongly coupled to translational/rotational motion of the OH^- or OD^-. The resulting anharmonic total-energy potential of these coupled motions decides by shape and relative depth of its single or double wells about the possibility of bistability, its thermal behavior, and the preference for B and R configurations in various hosts. [S0163-1829(96)03234-1]

I. INTRODUCTION

The F center in alkali halides is still *the* best investigated and understood isotropic one-electron defect in solids with strong electron-phonon coupling, serving as a *model system* for many theoretical concepts and for their experimental realization and tests.[1] Beyond this it is—due to its simple optically induced diffusion mobility—*the* most versatile building block, to construct much better than statistically defect pairs, -triples . . . , in order to study them optically and to develop them towards applications like tunable laser systems.[2] Besides pairs, triples . . . (F_2,F_2^+,F_3 . . .) formed by F centers themselves in pure crystals, many monovalent (Li^+,Tl^+,H^-,F^-) and divalent (Ca^{2+},Mg^{2+},Yb^{2+} . . .) point-ion impurities in doped crystals played an important role as pair partners of the F center. As the mass and binding force constant of these impurities are often quite different from the host ions they replace, the introduced *localized modes* and their coupling to the F electron are accessible for detection by Stokes resonance Raman scattering (SRRS), which helps to identify structure and symmetry of the defect pair.[3,4]

The discovery and intensive recent study of a class of defect pairs, formed by an F *center and a substitutional molecular ion* (like OH^-, CN^- . . .), has introduced interesting physical properties and application potential of these pairs, mostly called $F_H(OH^-)$, $F_H(CN^-)$ . . . centers. Their optical excitation in the electronic absorption (EA) leads to electronic-vibrational (E-V) *energy transfer* from the excited F electron into the vibrational stretch mode of the neighboring diatomic molecule under partial or total quenching of the normal electronic luminescence (EL).[5,6] Due to the very weak lattice coupling and long (10^{-3}–10^{-1} s) vibrational lifetime of CN^- molecular partners, this E→V transfer from F to CN^- can produce in some hosts efficient *vibrational luminescence* (VL), which led to first *vibrational superfluorescence and laser systems*.[7,8] Beyond this, the achieved population N_v of CN^- excited v states can easily and accurately be determined up to their third harmonic by anti-Stokes resonance Raman (ASRRS) experiments.[9] In contrast to this, the very high nonradiative relaxation rate ($\tau^{-1} \approx 10^9$ s^{-1}), measured for isolated OH^- defects[10] and expected to remain similarly high for F-OH^- pairs, makes direct energy-transfer observation from F to OH^- much more difficult: so far it has been detected only in two hosts CsI and KCl by very weak VL and ASRRS, respectively.[11,12] Strong quenching of the F-center electronic luminescence by neighboring OH^-/OD^- ions observed in many hosts,[13] shows indirectly that E→V energy transfer may be quite effective for these molecules as F-center partners.

Different from ''normal'' F aggregate centers which optically can be studied only by *electronic* absorption (EA), luminescence (EL), and Stokes resonance Raman (SRRS) spectroscopy, the F-center molecular pairs offer an important optical access: *vibrational* absorption (VA) and luminescence (VL) spectroscopy, which can be performed with high-resolution Fourier-transform (FTIR) technique. The molecular stretch-mode transition, mostly very sharp ($\lesssim$0.1–1.0 cm^{-1}) at low temperatures, is extremely sensitive to the perturbation and coupling introduced by the F-center neighbor: all its ''three lowest moments'' *oscillator strength, frequency position, and spectral width* can drastically change by the interaction effects. Detection of this ''*E-V perturbation*'' can be expected to be more informative about the coupled pair than the opposite ''*V-E perturbation*'' from the molecular oscillator on the strongly phonon-broadened electronic absorption band.

In this paper we study with combined EA and VA measurements the electronic and stretch-vibrational properties of $F_H(OH^-)$ and $F_H(OD^-)$ centers in KBr, KCl, RbCl, RbBr,

and RbI. It is well established from paraelectric work[14] that in all these five hosts the *isolated* OH^- molecular defects are $\langle 100\rangle$ oriented, reorienting rapidly by tunneling between the six equivalent minima of a rotational potential with barrier heights in the $\sim$700–2000 cm^{-1} range. The important question for the site symmetry of the closest possible F center/OH^- pair has been answered conclusively by electron-nuclear double resonance (ENDOR) experiments in KCl and KBr: in both these hosts the two partners are located on *next-nearest anion lattice sites*.[15] We expect (and this work will give more evidence for it) that this very general and unspecific $\langle 200\rangle$ pair model will be valid beyond KBr and KCl also in our newly studied three rubidium-halide hosts. Qualitatively, it is also safe to predict that the overall $\langle 100\rangle$ tetragonal symmetry of this defect pair will preserve for OH^- or OD^- its preferred $\langle 100\rangle$ orientations, but will split its sixfold degeneracy—due to strong elastic and/or electric distortions—into three levels: two single states of the OH^- molecule parallel to the pair axis (with its dipole moment pointing either towards or away from the F center), and a fourfold degenerate state of the OH^- orientation in the four $\langle 100\rangle$ directions perpendicular to the pair axis. Two possible OH^- orientational states and $\langle 200\rangle$ pair configurations are illustrated in Fig. 7 or KBr, discussed later in Sec. III. The resulting effective rotational energy potential should determine relative populations and reorientation rates among the unequal levels as a function of temperature for each host. Though population of only the lowest energy level could be expected for $T\rightarrow 0$ K, this will not be the case if large energy barriers prevent reorientation and achievement of Boltzmann equilibrium at lowest temperatures.

Such a *reorientational bistability* has in fact been found for *F* center-OH^- pairs in KBr and KI, first by magneto-optical experiments.[16] The two different configurations, observed to be stable at $T<10$ K, could be characterized by two different electronic absorption bands, slightly *red*- or *blue*-shifted relative to the normal *F* band. Though these ''*R*'' and ''*B*'' bands strongly overlap, they can by proper spectral photoexcitation become at least partially converted and reconverted into each other, i.e., *excitation of the F-center electron can change the orientational configuration of the neighboring OH molecule*. ENDOR experiments on the *F*-OH^- pair in KBr performed under this optical conversion have derived microscopic models for the two configurations,[15] which we will discuss in detail in Sec. III together with our results. Our experimental measurements (Sec. II) performed in five host materials (KBr, RbBr, RbI, KCl, and RbCl) have several objectives:

(a) To study with high-resolution FTIR the OH^- *stretching modes of stable or bistable pair centers* in spectral position, shape and strength between 4 and 80 K, and to correlate these VA results to the electronic EA properties.

(b) To determine from combined EA and VA absorption and conversion experiments the *absolute quantum efficiency* of the ''red to blue'' ($R\rightarrow B$) and ''blue to red'' ($B\rightarrow R$) photoconversion between the two configurations of bistable pairs.

(c) To derive from these optical (and from ENDOR) results *effective model potentials for the bistability*, based on translational/rotational motion and coupling of all important partners in the defect complex. Beyond this, the results of this study will supply a strong basis for the interpretation of ASRRS (Ref. 17) and short-time pump-probe[18] experiments in KBr:OH^- and KBr:OD^-, which have been running parallel to this work and are now being published together as three consecutive papers (I, II, and III).

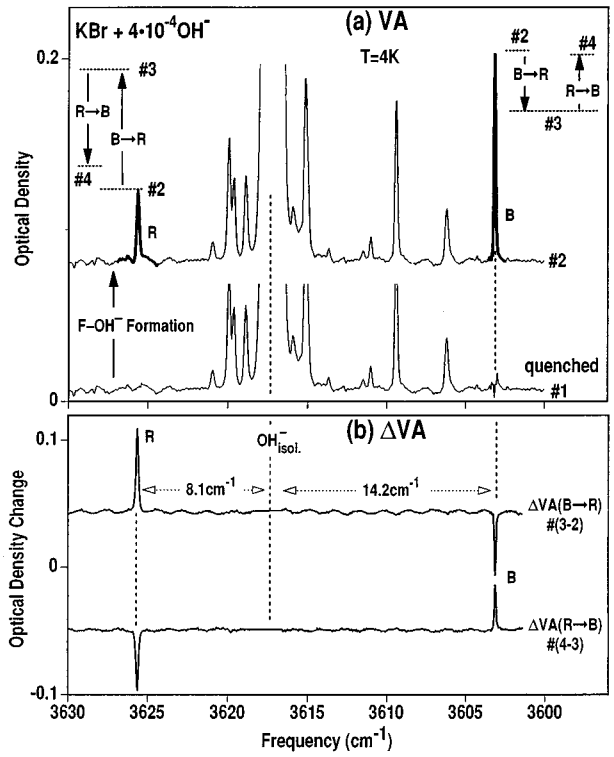

FIG. 1. Vibrational absorption (VA) and difference (ΔVA) spectra taken at 4 K in KBr:OH^- at four different stages (1–4): optical $F\rightarrow F_H(OH^-)$ aggregation (1,2) and subsequent $B\rightleftarrows R$ pair conversion (3,4), as explained in detail in the text.

II. EXPERIMENTAL RESULTS

A. Vibrational absorption (VA) measurements

The vibrational absorption (VA) was measured in a Bruker IFS88 Fourier-transform infrared (FTIR) spectrometer. In this instrument the optical pathway is computer controlled via moveable mirrors and hence allows a reliable switching between absorption measurements and irradiation of the samples with an external visible light source. For most sensitive detection we used difference spectra between measurements taken within a short time span before and after the light treatment. This method eliminates all uninfluenced absorption lines and most background interference effects so that absorption changes down to an optical density of 10^{-3} could be detected.

In Fig. 1 we show for an additively colored KBr+4×10^{-4} OH^- crystal the essential four-step procedure and information we obtain from high-resolution FTIR spectroscopy about the F-OH^- pair and its bistability. In the first step, the VA spectrum of the quenched crystal (1) at 4 K shows besides the strong (far off scale) ω_{01} absorption of isolated OH^- many sidebands, caused by OH^- ions which form pairs with other OH^- ions or with unwanted impurities like Na^+ ions; we neglect here these pairs, and will treat them in a

TABLE I. Fundamental 0→1 frequencies ω of the isolated OH^- or OD^- and the F-OH^- or F-OD^- centers in red (ω_R) and blue (ω_B) configuration, all given in cm^{-1} and ratio of vibrational oscillator strength (f_R/f_B). The last two columns give the ratios ([B]:[R]) determined in thermal equilibrium from VA spectra and after optimized optical conversion determined from the electronic absorption bands. All values determined at liquid-helium temperature (''4 K'').

Sample	ω (cm^{-1})	ω_R (cm^{-1})	ω_B (cm^{-1})	f_R/f_B	[B]:[R] thermal equilibrium	[B]:[R] after opt. conversion
KBr:OH^-	3617.4	3625.6	3603.2	2±0.5	4:1	2:3
KBr:OD^-	2668.3	2674.4	2658.5	3.3±0.5	8:1	1:7
RbCl:OH^-	3633.2	3640.5			>1:20	
RbBr:OH^-	3610.3	3618	3595.9	2.9±0.5	1:10	10:1
RbI:OH^-	3595.3	3600.5	3586.7	3.5±0.5	1:10	

separate paper.[19] After a second-step procedure (proper optical aggregation of the isolated F centers to OH^- defects at ~230 K and cooling without light to 4 K, two new sharp VA lines appear (spectrum 2) at 3603.2 and 3625.6 cm^{-1}, obviously related to the two bistable F-OH^- pair configurations. Their definite assignment to the pairs with the blue-shifted ''B'' or red-shifted ''R'' electronic absorptions is obtained in step 3 and 4 by optical conversion between both. As indicated by arrows, blue to red ($B\rightarrow R$) conversion of EA (by 565 nm irradiation) increases the high energy and decreases the low-energy VA line, while subsequent $R\rightarrow B$ conversion (by 642 nm irradiation) produces the opposite.[20] In Fig. 1(b) these two optical conversions are shown not as a VA but as a ''ΔVA difference spectrum'' between both processes. Removing common noise and interference effects and totally eliminating all absorptions which are not altered, they show the positive and negative ΔVA ($B\rightarrow R$) and ΔVA ($R\rightarrow B$) changes. Obviously the high-energy VA line must be assigned to the electronic R absorption, the low-energy VA line to the B absorption. Besides exact frequency positions ω_R and ω_B from these ΔVA spectra, integration over their positive and negative parts yield accurate values of the relative oscillator strengths ratio f_R/f_B. By similar measurements like in Fig. 1 for KBr:OD^- crystals (not shown here), these values were determined also for F-OD^- pairs, and are summarized (together with other quantities) in Table I.

Host material variation to RbBr and RbI yielded rather similar results about the low-temperature bistability of the $F_H(OH^-)$ centers as obtained for KBr. First their EA absorptions showed blue- and red-shifted F_H bands which could be used for optical $R\rightleftarrows B$ conversions at $T=4$ K; (details about the EA bands and the used conversion wavelengths will be discussed in Sec. II B). The VA and ΔVA responses of the bistable R and B configurations in these hosts were measured with exactly the same four-step process as shown and explained above in detail for KBr:OH^-. In the rather low-doped RbI:OH^- (Fig. 2), two sharp lines (at 3600 and 3587 cm^{-1}) appear after $F\rightarrow F_H(OH^-)$ conversion on both sides of the OH^- stretchband, with considerably smaller spectral separation compared to KBr:OH^-. By successive $B\rightarrow R$ (step 3) and $R\rightarrow B$ (step 4) EA conversions their assignments to the bistable B and R configurations can be made, as shown in Fig. 2. For RbBr:OH^- the VA result looks ''on first sight'' somewhat different (Fig. 3), because only a single strong and sharp lines appears after $F\rightarrow F_H$ conversion on the high-energy side (at 3618 cm^{-1}) of the OH^- stretchband in step 2. However this line reduces strongly under EA $R\rightarrow B$ conversion and a new line appears at 3595 cm^{-1} (step 3) which can be $B\rightarrow R$ back converted in step 4. For both RbI:OH^- and RbBr:OH^-, the lower parts of Fig. 2 and 3 show very accurate ΔVA ($B\rightarrow R$) and ΔVA ($R\rightarrow B$) difference spectra of the optical conversion processes. The resulting ω_R and ω_B values and the f_R/f_B ratios are summarized in Table I.

In contrast to these ''positive VA results'' on the existence of F-OH^- bistability in KBr, RbBr, and RbI, there are two ''negative'' ones, both in alkali-chloride hosts. The first case is RbCl:OH^- which shows after $F\rightarrow OH^-$ aggregation the appearance of a single VA line on the high-energy (R) side at ~3640 cm^{-1}. In spite of several attempted irradiation into the red or blue side of the electronic absorption (600–

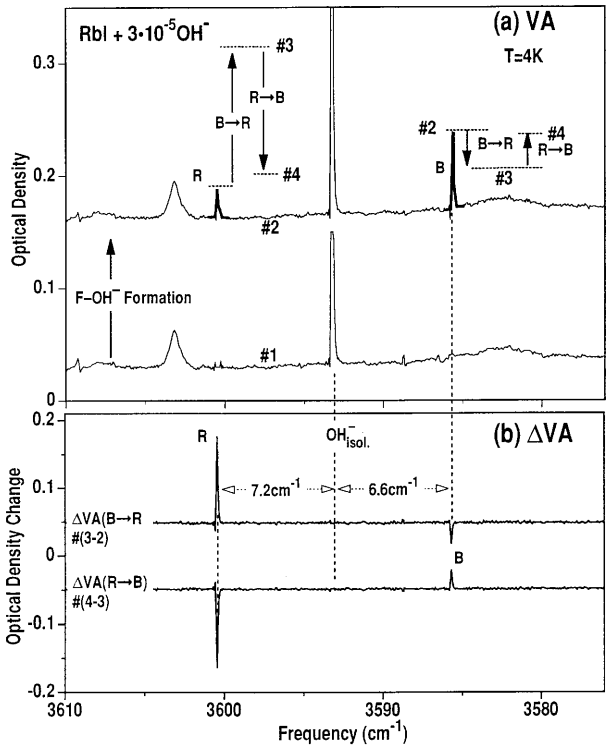

FIG. 2. Similar VA and ΔVA spectra like in Fig. 1 measured at four different stages for RbI:OH^-.

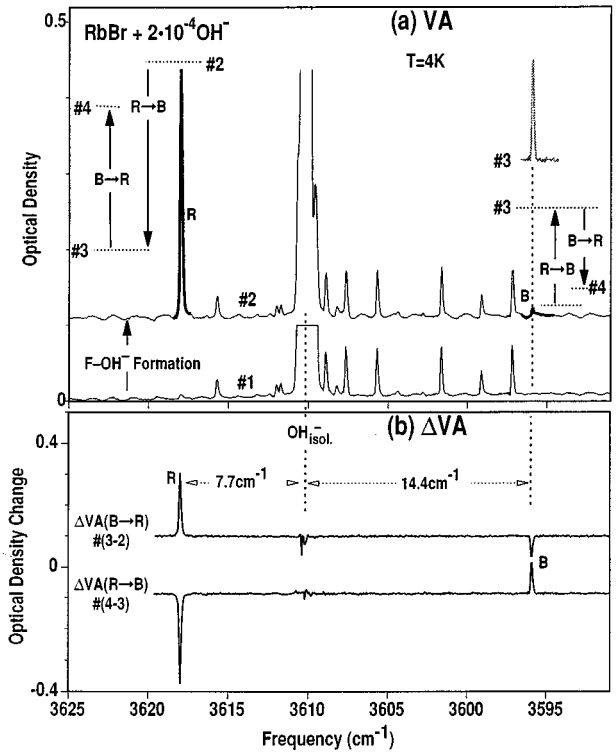

FIG. 3. Similar VA and ΔVA spectra like in Fig. 1, measured at four different stages for RbBr:OH^-.

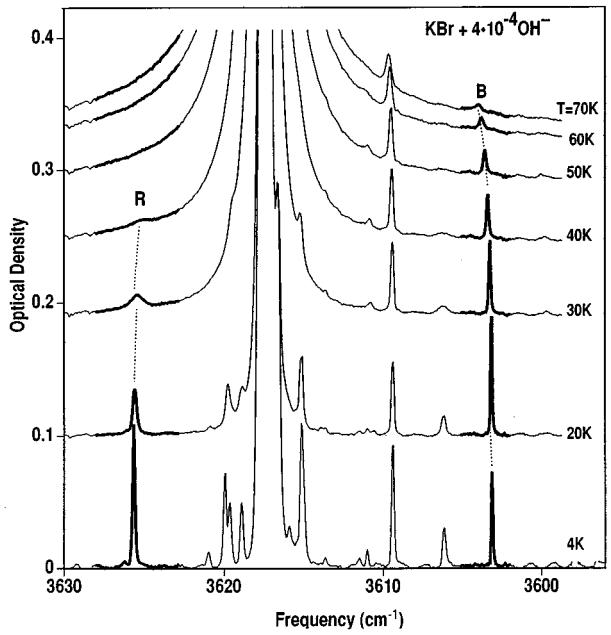

FIG. 4. VA spectrum in KBr:OH^- from Fig. 1 after optical $B \rightarrow R$ conversion (stage 3) under variation of temperature 4–70 K.

700 nm) at 4 K, neither this line decreases nor a new one appears. This clearly indicates true stability for only one single R configuration; any possible alternative B configuration produced by optical pumping, must have even at 4 K a high thermal decay rate, at least more rapid than the minimum time needed (~1 min) to run a VA spectrum.

Even more negative is our VA result in KCl hosts. In spite of repeated experiments in low ($\sim 10^{-4}$) and high ($\sim 10^{-3}$) doped crystals, not any VA line could be observed after $F \rightarrow OH^-$ aggregation, neither on the high- nor the low-energy side of the isolated OH^- stretch absorption. We will discuss this negative result in Sec. III.

For all the four hosts with bistable or stable $F_H(OH^-)$ VA lines we measured accurately the *temperature variation* of their VA spectra. As one example, Fig. 4 shows for the $F_H(OH^-)$ pairs in KBr the VA spectra after optical $B \rightarrow R$ conversion in a temperature range between 4 and 70 K. Neglecting again all other sidebands and focusing on our R and B lines, we see some clear trends with rising temperature: both lines broaden (stronger for R than for B), reduce a bit their splitting from the frequency of isolated OH^-, and decrease strongly their integrated intensity. These general trends can be observed in a similar way for the RbCl, RbBr, and RbI hosts.

Careful integration of the VA lines B and R yields for each of these hosts the B and R absorption strength as a function of temperature. Using for the bistable systems their measured oscillator strength ratio f_R/f_B from Table I (which we assume to be T independent), we can ''translate'' the measured B/R *absorption strength ratios* into the $[B]:[R]$ *concentration ratio*. Values of these ratios measured at 4 K are summarized in Table I. In Fig. 5 the temperature depen-

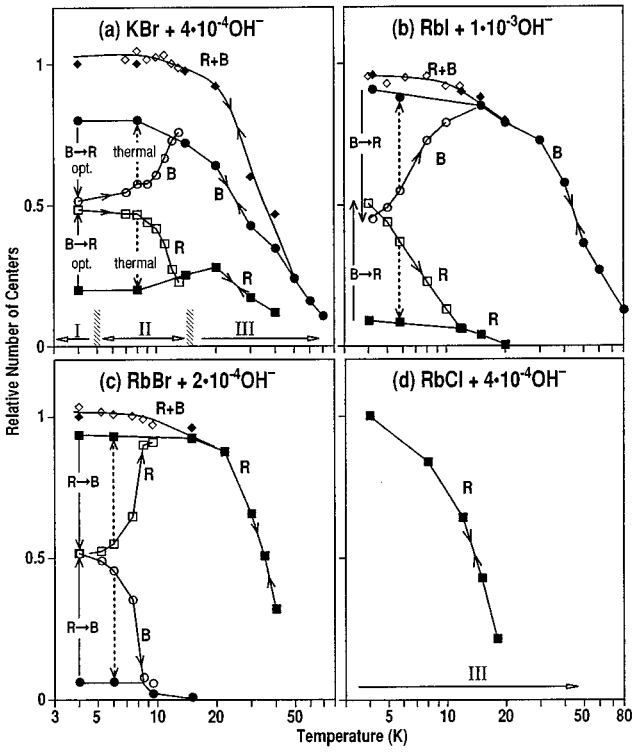

FIG. 5. Relative number $[B]$ and $[R]$ of $F_H(OH^-)$ centers in B and R configurations as a function of (logarithmically plotted) temperature in four hosts (a) KBr, (b) RbI, (c) RbBr, (d) RbCl measured by their VA absorptions in two ways: (A) Reversible thermal cycle $80 \rightleftarrows 4$ K without optical conversion (● and ■). (B) Interruption of the same cycle at 4 K by optical conversion at 4 K, and subsequent heating in the dark (○ and □). The summation of centers $(R+B)$ is indicated as ♦ for cycle (A) and as ◇ for cycle (B).

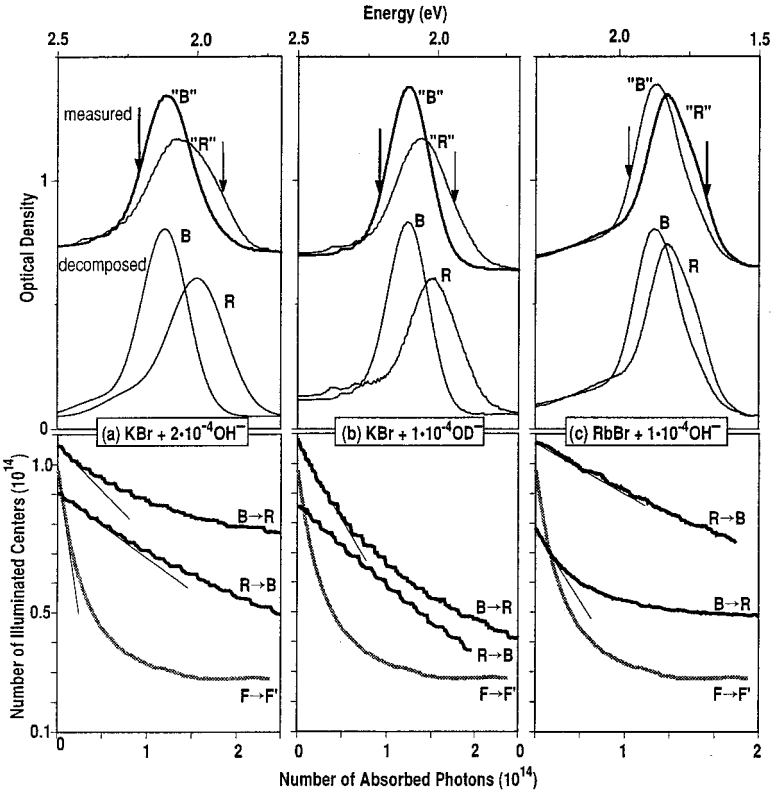

FIG. 6. Summary of electronic absorption and optical conversion properties at 4 K of F_H centers in (a) KBr:OH^-, (b) KBr:OD^-, and (c) RbBr:OH^-. Upper part: the first row shows for each case the best experimentally achievable (but still ''composite'') measured ''*B*'' and ''*R*'' bands, and below this their constructed decomposition into the ''true'' *B* and *R* bands, as described in text. Lower part: EA conversion curves between *B* and *R* centers in comparison to $F \rightarrow F'$ conversion (at 100 K and 560 nm in KCl). For details see text.

dence of the relative $[B]$ and $[R]$ concentration is depicted in four different hosts (a)–(d) for measurements obtained by two different procedures: the full symbols (● and ■) indicate *R* and *B* values obtained in a reversible closed thermal cycle $80 \rightleftarrows 4$ K without any optical light irradiation and conversion; the open symbols (○ and □), indicate interruption of this cycle after cooling, optical conversion at 4 K ($B \rightarrow R$ for KBr and RbI, $R \rightarrow B$ for RbBr hosts), and subsequent continuation of the thermal cycle $4 \rightarrow 80$ K without further light irradiation. For all three bistable systems, the changes which were induced by light in the lowest temperature range I [$T<5$ K, indicated for KBr in Fig. 5(a)] disappear in a *T*-range II ($5<T<12$ K), such that above $T \approx 12$ K the values of closed and interrupted cycles become again identical. The measurements on the branches of the interrupted cycle were obtained in consecutive order under increase of *T* within a time as short as possible (5 min) without allowing the system to reach its thermal equilibrium. Under repetitive VA measurements at a constant temperature, on the other hand, the *R* and *B* numbers return to a thermal equilibrium distribution (as indicated in Fig. 5 by dashed arrows), which is identical to the one observed during cooldown. The rate of reaching the equilibrium increases rapidly with *T* (e.g., for KBr:OH^-, ~30 min at $T=5$ K, <1 min at $T=12$ K). This shows that long time bistability is only present in the temperature range I. Regardless of how the changes in the relative $[R]$ and $[B]$ concentration are obtained, the $(R+B)$ summation below 8–12 K becomes nearly temperature independent and is shown in Fig. 5 to be (within experimental error bars) identical for both the closed (♦) and interrupted cycle (◇). This confirms the validity of our assumed temperature independence of f_R/f_B (determined at $T=4$ K)—at least in the low-*T* ranges I and II. For temperatures above $T \approx 14$ K (range III) the sum of $R+B$ gradually disappears for all four hosts.

In summary of our VA results (mostly shown in Figs. 1–5), some important similarities (i) and differences (ii) in the behavior of the bistable systems in KBr, RbI, and RbBr should be emphasized:

(i) In all three cases, the VA_R and VA_B line frequency shift $\Delta\omega$ from the OH^- stretchband lie in their directions opposite to the blue- and redshift of their electronic transitions; the VA_R line has considerably higher oscillator strength and temperature broadening compared to VA_B). After translation of their strength into $[B]$ and $[R]$ concentrations, the sum $[B]+[R]$ is nearly constant below $T \approx 14$ K (independent of thermal cycling or any optical conversions), while for $T>14$ K it decays drastically and disappears in all three cases in the $T \approx 50-80$ K regime.

(ii) Only details of their preference for the *B* or *R* configurations are quite different: For KBr:OH^- the $[B]:[R]$ ratio at 4 K is 4:1 and decreases towards 20 K to about 2:1. For RbI:OH^- the $[B]:[R]$ ratio at 4 K is a bit higher ≈10:1, and increases towards 20 K to a higher value (hard to determine due to the small size of $[R]$). For RbBr:OH^- the $[B]:[R]$ ratio at 4 K lies opposite ~1:10 and decreases even more under temperature increase.

B. Electronic *R* and *B* absorption and conversion quantum efficiency

Though $B \rightleftarrows R$ photoconversions have played *the* major role in our assignment of two observed VA lines to the *R* or *B* configurations, we have not yet shown the relevant electronic absorption EA spectra and optical conversion efficiency. We have studied these features in detail for the three bistable KBr:OH^-, KBr:OD^-, and RbBr:OH^- systems, and summarize in the comprehensive Fig. 6 the essential results, (all at $T=4$ K). The samples were chosen to study both the

influence of host and isotope variation. In the upper horizontal row we show the best achievable separated ''*B*'' and ''*R*'' absorption bands, one of them (thicker line) obtained for each system by the thermal equilibrium at 4 K. The other configuration (not favored by thermal occupation), can only be accumulated by full optical conversion at 4 K into saturation under irradiation with best chosen wavelength (indicated by thicker arrows). The optical conversion achieved in our EA studies were more complete than the corresponding ones in VA because thinner samples with lower EA bands were used. It is obvious from our VA result that always both *R* and *B* configurations are present and for that reason our ''*R*'' and ''*B*'' spectra can only represent a composite of true *R* and *B* absorption curves. We performed a decomposition of our EA bands using the thermally achieved $[B]:[R]$ ratios determined from VA. These concentration ratios are naturally identical for VA and EA and could be used unmodified because (different than in VA) they are equal to the electronic *B* and *R* absorptions strength ratios. This additional information removes most of the uncertainty of earlier decomposition attempts solely based on EA results.[21]

Decomposition of the EA bands is most easy in the RbBr:OH^- and KBr:OD^- systems for which the thermal equilibrium favors one specific configuration. Moreover, a rather complete optical conversion could be achieved which simplified our fitting procedure even more. The resulting absorption band of the ''pure'' *R* and *B* configuration which are only slightly different from the measured ones are shown in Fig. 6 on the bottom of the upper horizontal row. The determined concentration ratios after complete optical conversion are included in Table I. They are approximately just opposite to the ones found in thermal equilibrium. For KBr:OH^- the decomposition was more difficult due to its much stronger mixed (4:1) ratio in thermal equilibrium. Several iterative fitting steps were necessary to obtain good unambiguous fits (Fig. 6). Even more than for the ''*B*'' band we found within the photoconverted ''*R*'' band a very strong mixture ($[B]:[R]=2:3$). In KBr, there is a significant difference between the OH^- and OD^- isotopes in their concentration ratios both before and after optical conversion. Taking this into account, the notable differences in the measured OH^- and OD^- absorption spectra ''*R*'' and ''*B*'' can well be accounted for. The decomposed *R* and *B* band shapes become within the experimental uncertainties almost isotope independent.

The most difficult experimental task was the determination of the $B\rightarrow R$ and $R\rightarrow B$ conversion absolute quantum efficiency, which we performed for KBr:OH^-, KBr:OD^-, and RbBr:OH^-. Both the spectral EA measurements and the optical conversions were performed and detected with the stabilized light source of our Cary 17D spectrophotometer. Tuned to the appropriate wavelength for conversion, its irradiated intensity was used both for photoconversion and photodetection of the optical density change in time. It has been shown that the initial slope of such decay curves is proportional to the conversion efficiency as long as one excites in the beginning dominantly the defect to be bleached. It can be seen from the EA spectra in Fig. 6 and the indicated position for the conversion wavelength that the latter condition is fulfilled reasonably well for our samples. In order to obtain from the directly measured optical density versus time curves the desired absolute quantum efficiencies of the conversion both coordinate axis have to be calibrated:

(1) The time axis has to be expressed in terms of the *number of incident or absorbed photons*.

(2) The measured absorption has to be expressed in terms of the *number of absorbing centers*.

Evaluation (1) was achieved by comparing under the same conditions of light source and instrumental detection our curves directly with the $F\rightarrow F'$ conversion in KCl, which has at $T=100$ K the well-known quantum efficiency of about 2. This ''calibration'' was done at one particular spectral position which coincides with the position of the $B\rightarrow R$ conversion in KBr. The photon numbers at other wavelengths were determined by measurement of their relative light intensities with photon counting (PbS or Si) light detectors. Some complication is introduced by the fact that the portion of the incident photons which is absorbed by the sample reduces during the conversions. However, we are mainly interested in the initial slope and therefore could neglect this effect in our calibrations. The fraction of the absorbed photons is then determined by the initial optical density of the sample at the irradiation wavelength. The center numbers (evaluation 2) were determined by evaluating the whole spectral absorption curves and using the Smakula's formula. The absorption strength at one particular spectral position represents the number of centers as long as no other absorption overlaps. In our measurements this is only approximately the case at $t=0$ while for later times the other type center appears as a growing overlapping absorption. For this reason our measured decay curves shown in the lower part of Fig. 6 do not go to zero even if the conversion is almost complete. Again, using only the initial slopes, minimizes the introduced error ($<10\%$). We tested the whole method by measuring the back conversion $F'\rightarrow F$ at 4 K and obtained an accuracy of $\pm 10\%$. The corrections (1) and (2) are already included in the presentation of the experimental results in the lower part of Fig. 7. We included for each graph also our measured $F\rightarrow F'$ result. In this way a convenient comparison is possible and the absolute quantum efficiencies can be obtained directly from the initial slopes which are summarized in Table II. Realistically, there is a considerable uncertainty in these values due to the sum of possible errors within the described multistep evaluation process. For this reason we quote the η within an estimated error bar. However, this does not change our most basic and important result: *The absolute quantum efficiency is high* ($\sim$20–60 %) *in all cases, independent of host, isotope, and [B]:[R] variation*. It appears that the quantum efficiencies η for RbBr:OH^- and KBr:OD^- are higher compared to KBr:OH^-. However, we suspect that the η values might be underestimated in KBr:OH^- due to the fairly strong spectral overlap of the ''*R*'' and ''*B*'' EA bands.

III. DISCUSSION AND INTERPRETATION OF RESULTS

In this section we try to interpret our EA and VA static and dynamic results and establish relations to microscopic models for the F-OH pair. We start out with a review of the ENDOR results which are among the bistable systems only available for KBr and try to correlate them to our optical results. In the ENDOR/ODENDOR experiments performed in KBr,[15] several new resonance lines appeared or changed

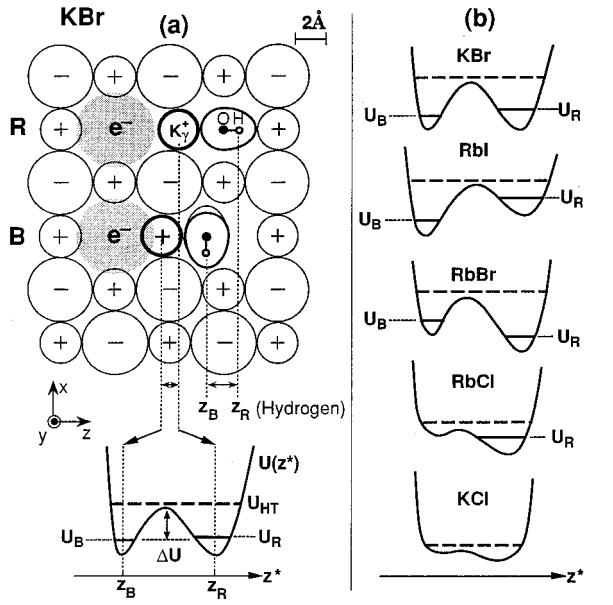

FIG. 7. (a) View of a (100) plane in KBr showing in proper size and positions the three constituents of the $F_H(OH^-)$ center complex in their R and B configurations as determined by ENDOR. The bottom part shows in a five times expanded scale the off-center positions z_B and z_R, and schematically an effective energy potential $[U(z^*)]$ for the K_γ^+ cation. (b) Schematic $U(z^*)$ potentials for KBr, RbI, RbBr, RbCl, and KCl derived from VA results. For details and discussion see text.

under optical $F \rightarrow F_H(OH^-)$ and subsequent $B \rightarrow R$ conversion; (among them were lines from the hydrogen nuclei of OH^- molecules, whose oxygen cannot be detected due to nearly absence of the magnetic ^{17}O isotopes). Analysis of values, signs, and symmetries of the measurable superhyperfine (SHF) interaction tensors yielded—besides the general (200) site symmetry of the F-OH^- pair—more detailed informations about the nuclei of hydrogen and the nearest-neighbor (NN) K_γ^+ ion located on the pair axis between the F center and OH^- defect. In Fig. 7(a) these microscopic details are illustrated as clear as possible with a view on the (100) plane of KBr, drawn with proper sizes of host ions[22] and the OH^- molecule.[23]

(a) In the *R configuration*, the distances of the K_γ^+ and the H nuclei from the F electron are found to be 3.8 and 7.4 Å, respectively, showing for both of them a considerable large (~0.5 Å) *increase* compared to their normal lattice positions. The observed positive sign of both the isotropic and anisotropic hydrogen SHF interaction indicates alignment of the OH^- molecule parallel to the ⟨200⟩ defect axis. As shown for R in Fig. 7(a) with the proper determined K_γ^+ and H distances, this allows for spatial arguments only a model with the hydrogen part of the OH^- pointing away from the F center. Moreover, gain in electric dipole interaction energy by the parallel oriented K_γ^+ displacement and OH^- molecular dipole vector will favor this configuration.

(b) In the *B configuration*, the distance of the K_γ^+ and H nuclei from the F electron are found to be 2.8 and 5.4 Å, respectively, showing for both of them (in contrast to R) a large *decrease* compared to the normal lattice positions. Similarly in contrast to R, a negative sign of the hydrogen isotropic SHF parameter has been observed for B, understandable so far only on the basis of exchange polarization effects.[24] This requires OH^- orientations perpendicular to the pair axis yielding with proper distances the B structural model in Fig. 7(a). As the lower symmetry of this arrangement is not observed in ENDOR, a rapid ($\tau^{-1} > 10^6$ s) center OH^- reorientation within the xy plane has to be assumed.

Based on these ENDOR results it is easy to understand qualitatively why the observed shifts of the OH^- vibrational lines in KBr (Fig. 1) are opposite in direction to the shifts of the corresponding EA bands (Fig. 6). For both the EA and the VA positions exist empirical rules which predict that the transition energy increases with a decrease in the average distance d to the neighbors. While for the F electron absorption this rule is expressed as the well known Mollwo-Ivey relation[25] $E \propto d^{-2}$, it is well established for the OH^- vibrational absorption from uniaxial stress experiments,[26] host material variation, and theory,[27] that, e.g., a reduction of d leads due to increasing repulsion to a higher VA transition energy. Both together explain the observed behavior considering that the off-center shifts of the K_γ^+ ion between the F-OH^- pair, have opposite effects on the two partners: ''more space for the F center'' means ''less space for the OH^- ion,'' and of course vice versa. This relation between spectral position shifts is shared by all the bistable systems that we studied (KBr:OH^-, KBr:OD^-, RbBr:OH^-, RbI:OH^-) so that we assume (in spite of the absence of ENDOR result), that similar R and B type configurations exist, characterized by strong off-center positions of the cation between F center and OH^-. Even in RbCl, the single observed EA and VA bands exhibit opposite shift and establish the one stable pair-structure to be an R configuration. Beyond these very plausible general trends of EA and VA frequency shifts, it is much harder to understand and answer more detailed questions, for instance: Why does the very large (~16%) inward or outward shift of only one of the six cation neighbors of the F center not lower the symmetry enough (like for F_A centers) to split the EA transitions for polarization parallel and perpendicular to this strong ungerade perturbation? Besides a slight indication for some inhomogeneous broadening in the R band of RbBr, none of this is apparent in the decomposed B and R bands of KBr (see Fig. 6). Without any theoretical justification one has obviously to assume, that the low defect symmetry (produced by a very strong ungerade distortion from the NN K_γ^+ shift) becomes somehow ''averaged out'' over all coordinates, so that a

TABLE II. Absolute quantum efficiencies η measured at 4 K for $R \rightarrow B$ and $B \rightarrow R$ conversion of F-OH^- or F-OD^- centers in KBr and RbBr.

System	$\eta_{R \rightarrow B}$	$\eta_{B \rightarrow R}$
F-OH^- in KBr	0.2 ±0.1	0.31±0.1
F-OD^- in KBr	0.32±0.1	0.57±0.2
F-OH^- in RbBr	0.21±0.1	0.51±0.2

nearly isotropic and homogeneously broadened transition results for both R and B.

The ENDOR results reviewed above make it obvious that our defect complex is not properly described as a simple F-OH^- pair on next-nearest-neighbor (NNN) anionic lattice sites, but that the NN cationic ion located between these two partners plays a decisive role for the statics and dynamics of the bistability. In Fig. 7(a) we have indicated by dotted lines the nearly symmetric ± 0.5 Å shift of this K_γ^+ ion from its normal position. Expanding in the lower part of Fig. 7(a) this $\Delta z = 1$ Å separation of the dotted lines by a factor of 5, we draw a schematic potential $U(z)$ for the K_γ^+ ion in which at $T < 10$ K it occupies the shifted positions z_B and z_R. In contrast to the quasiharmonic single-well potential of a normal K^+ ion in the perfect lattice, this shallow two-well (or ''off-center'') potential $U(z)$ is created by the presence of two different substitutional defects on both opposite NN sites along the z direction of the K_γ^+ ion:

(i) The highly polarizable and ''soft'' $1s$ electron of the F center on the left side, which allows, e.g., easy motion of the K_γ^+ ion towards it without ionic repulsion. As a possible change of its $1s$ wave function is quite small (no shift from the vacancy center was detected by ENDOR) in the B and R configurations, we consider its position—as drawn in Fig. 7(a)—as constant.

(ii) The OH^- molecular partner on the opposite NN site of K_γ^+ is characterized besides its electric dipole by highly nonspherical contours of its shape with much smaller dimensions than the spherical Br^- ion it replaces [properly drawn in Fig. 7(a)]. Even as an isolated defect, this large size-misfit allows besides rotation also translational motion of the OH^- between off-center positions in the large Br^- vacancy, thus affecting by interaction the temporary positions of its six equivalent NN cation neighbor. This ''dressing-effect'' slows down by an increased ''effective moment of inertia'' the OH^- tunneling-reorientation,[28] but permits for free OH^- in KBr still a rate of about 10^5 s^{-1} at 4 K. The drastic increase in the range of positions of one particular NN cation K_γ^+ (made possible by a soft F center on its other side) leads to strongest enhancement of the dressing effect by its localization on this particular ion. For two extremely large ± 0.5 Å shifts of this mobile cation neighbor, two particular OH^- ion positions and orientations become stabilized at low temperatures: total parallel alignment along the z axis for the R configuration, and perpendicular alignment for B permitting rapid reorientation in the xy plane around the axis of the strong K_γ^+ dressing effect.

Summarizing this we realize that our plotted $U(z)$ energy curve in Fig. 7(a) should not be regarded as describing only the linear z motion of the K_γ^+ ion in a ''fixed environment.'' If one would assume that both F center and OH^- neighbors remain totally constant and unchanged, a two-well potential may not even exist for the z motion of the K_γ^+ ion. This potential is mostly created by the fact that under z shifts of K_γ^+ from its normal position in both opposite z directions, the internal energy of the total system becomes first lowered by particular translational-rotational motion of the OH^- ion on one side, and changes of the energy of the F-center $1s$ ground state on the other side. For further increasing K_γ^+ shifts, the internal energy will increase again, thus creating the resulting double-well potential. The complexity of all detailed interactions prevents at presence any comprehensive description of the total system by a multicoordinate energy surface model. Instead of this we still use for convenience the simplified description with a single coordinate for the K_γ^+ linear displacement indicating its much more generalized coupled nature by the notation z^*. It should always be kept in mind that for each z^* value a different position and reorientational behavior of the OH^- will exist. For instance at z_R the OH^- is orientationally aligned, while it performs at z_B rapid rotating around the z axis in the xy plane. In terms of this description it is evident that bistability of our linear three-defect (F-K_γ^+-OH^-) system at low temperature will only occur, when the $U(z^*)$ potential shows two deep enough wells in which the lowest eigenstate lie well below the separating energy barrier ΔU. Though this looks a bit similar to the situation of off-center point-ion defects (like Li^+ in KCl), there is an important difference: the latter are described due to their symmetry in cubic lattices by tunneling states of the point-ion in an equal multiwell potential, which becomes unequal (and localizes the states) only by applied or internal background- stress or electric fields. For our K_γ^+ ion with two totally different (F and OH^-) neighbors and interactions or couplings on both sides, the ''off-center potential'' $U(z^*)$ will always be totally unsymmetric in terms of depth and width of the two minima, as indicated schematically for KBr in Fig. 7(a). The lowest U_R and U_B states in these two wells must be regarded (even if they have accidentally the same energy) as localized states of two different coupled K_γ^+-OH^- pairs, which can change positions between the U_R and U_B minima only by thermally activated motion over the barrier under gradual (adiabatic) change of their coupling character from the R to B configuration. Besides the U_R and U_B ground states, excited states due to K_γ^+-OH^- motions (or modes) can exist in the two potential wells. Due to perpendicular (B) or parallel (R) OH^- orientation relative to the z direction of K_γ^+ motion, coupling nature and strength ''z'' of the K_γ^+-OH^- pair and its modes can be very different in the B and R potential wells.

It is evident from the above discussions, that the $U(z^*)$ potentials of our strongly coupled three-defect system will be extremely sensitive to any change of its constituents and the lattice entities and spacings. For the five hosts we studied, variation of lattice parameter changes strongly the $\langle 200 \rangle$ F center/OH^- distance, the anion $Cl^- \rightarrow Br^- \rightarrow I^-$ variation the space available for the OH^- off-center shifts, and cationic $K^+ \rightarrow Rb^+$ variation both size and electronic polarizability of the important off center cation in the middle. Due to the absence of any theoretical treatment for interpretation of our experiments, we try the opposite approach: using our VA(T) results from Figs. 1–5 to approximately predict $U(z^*)$ potentials, and to establish phenomenological trends under host and temperature variation which may provide guidelines for later theoretical treatments. In order to avoid thermal population of any higher lying translational/rotational energy levels, we consider first the lowest temperatures $T < 5$ K [indicated as range I in Fig. 5(a)]. In clear contrast to our two studied chloride hosts KCl and RbCl (which we treat later), we detect in KBr, RbBr, and RbI hosts at 4 K two sharp VA lines oppositely shifted from the free OH^- VA line, which definitely show (together with their shifted EA absorptions) the presence of two thermally stable R and B configurations.

The large misfit of the Br^- and I^- anion sizes compared to the small OH^- obviously permits easy off-center shifts of both the OH^- and the K^+_γ or Rb^+_γ cations and creation of $U(z^*)$ potentials with the distinct minima. The shape of this potential can be obtained from the detected $[B]$:$[R]$ thermal equilibrium measured at 4 K after cooling without optical conversion (see Fig. 5 and Table I). The opposite 1:10 and 10:1 ratios observed for OH^- in RbBr and RbI hosts, respectively, leads in our descriptive model to potentials with opposite relative U_R and U_B energies as drawn schematically in Fig. 7(b). It is interesting to note that ''in between'' these two cases of oppositely shaped potentials appears to lie KBr:OH^- which shows both B and R configurations in substantial amounts. Assuming that its 4:1 concentration ratio observed at lowest temperature is based on the multiplicity ratio of 4:1 of the B and R configurations (as postulated by the ENDOR model), a rather symmetrically shaped $U(z^*)$ potential with $U_R \approx U_B$ will result, as depicted in Fig. 7. Besides this host material dependence, the potential $U(z^*)$ also shows a quite significant change under isotope variation: In contrast to the KBr:OH^-, we observed in the KBr:OD^- case (at low T) a clear preference for the B configuration suggesting a double-well potential with $U_B < U_R$ [more similar to the one depicted in Fig. 7(b) for RbI]. Obviously, differences in vibrational or translational-rotational motion between the two chemically and in size quite similar isotopes, play also a role in determining the potential.

Under temperature increase into range II ($5\ \mathrm{K} < T < 15\ \mathrm{K}$) we find in all our bistable cases that optically produced changes in the $[B]$:$[R]$ ratio disappear with a rate gradually increasing with T, returning the system into thermal equilibrium without any loss in the sum of $B+R$ [see Figs. 5(a)–5(c)]. Though we still regard to remain in our model potential at $kT < \Delta U$, thermal activation energy can achieve now translational/rotational transitions over the energy barrier between the two configurations. For RbBr and RbI with their very unsymmetric potentials we can observe this thermally induced transitions after optical conversions only from the higher shallow into the lower preferred well. The most interesting behavior is again exhibited in KBr:OH^-. In this host we observed, besides the start of thermal reorientation, a change in the thermal equilibrium of the $[B]$:$[R]$ ratio from 4:1 at $T=4$ K to 2:1 at $T=15$ K. It appears that even the double-well potential itself is a bit temperature dependent, making the red configuration more favorable towards higher T. The fact that this change is reflected in the center numbers indicates that not only $R \rightarrow B$ but also $B \rightarrow R$ thermal conversion can take place in this T-range II, supporting our assumption that $U_R \approx U_B$.

Under further increase of temperature into range III ($T > 15$ K) we observe in all bistable cases a gradual disappearance of both VA_B and VA_R lines—without appearance of any observable new VA lines (see Figs. 4 and 5). This strongly indicates a gradual transition into a new ''high temperature (HT) phase'' of our three-defect system. In terms of our $U(z^*)$ model, we assume that we thermally occupy now with increasing probability states lying above the energy barrier ΔU of the shallow two-well potential (indicated as U_{HT} schematically by dashed lines in Fig. 7), so that the K^+_γ (or Rb^+_γ) ion becomes less off-center located at z_R and z_B, but more and more free to perform linear vibration over the whole available z range of the anharmonic potential. As a consequence of such K^+_γ (or Rb^+_γ) vibrations, the OH^- ion undergoes drastic changes in both its axial position and its reorientation behavior. The new ''averaged'' K^+_γ (or Rb^+_γ) position, which lies somewhere around the center of the potential, yields for the OH^- molecule a situation more resembling the one it encounters as isolated defect with similar expected reorientational behavior and oscillator frequencies. For these reasons, the VA response of the system in this high-temperature state ''VA_{HT}'' will no longer consist of two shifted and sharp lines, but will be hidden in rotationally broadened form under the inevitable and much stronger isolated OH^- absorption band making it ''invisible'' for our studies. (We still plan to do most sensitive experiments trying to make it ''detectable''). Because states above the barrier become only gradually thermally populated, the transition from the distinct R and B configuration into the new ''high-temperature phase'' of our complex will be gradually, as we observe in the disappearance of $VA_B + VA_R$ (see Fig. 5).

This characterization of our bistable systems and their T dependence by three different VA lines should in principle be possible similarly for three electronic absorptions EA_B, EA_R, and EA_{HT}. However, in drastic contrast to the spectrally well separated VA lines, the broad bands of the phonon-coupled EA transitions strongly overlap, a problem which badly increases with T due to further individual temperature-broadening and shifts of each of the three components. At least at lowest T (range I), the existent $EA_R + EA_B$ composite band can be well separated using the optical conversion process (see Fig. 6); in range II up to $\sim$15 K it still remains a $R+B$ composite bands with proper $[B]$:$[R]$ thermal equilibrium, reflecting by its shape the sum of their temperature broadenings and shifts. The biggest change is expected in range III (>15 K) in which EA_R and EA_B should gradually decrease (similar as seen for VA in Fig. 5) and become replaced by the EA_{HT} band. One ''advantage'' of the EA_{HT} absorption (compared to the hidden VA_{HT}) is the fact that it is basically fully detectable at high enough temperatures. In all so far studied bistable systems EA_{HT} lies on the low-energy side of the F band,[13,16] which often has been used to explain it as an R configuration.[15,16] We interpret EA_{HT} very differently (as discussed above for VA) as an F-center transition perturbed by the presence of an NN cation with large amplitude linear vibration and a $\langle 200 \rangle$ neighboring rapidly rotating OH^- molecule. The always observed low-energy shift compared to F makes very much sense, because due to the smaller size of reorienting OH^- compared to the anion size it is expected that the K^+_γ (or Rb^+_γ) ion will be shifted away from the F center [as indicated schematically by the unsymmetry of the $U(z^*)$ potential in Fig. 7].

While in the alkali-bromide and iodide host materials discussed so far a fairly large size misfit between host cation and the OH^- exists and allows bistability, this misfit is much smaller in the alkali chlorides (KCl, RbCl) and makes it much harder for the K^+_γ or Rb^+_γ to create two (or even only one) stable off-center positions. In RbCl:OH^- we observe only a single VA_R line at 4 K, with no ability for optical

$R \rightarrow B$ conversion and with rapid decay in strength under rising temperature, reaching zero at $T = 20$ K. In the smaller lattice parameter host KCl, not any detectable VA_R and VA_B line can be observed (in spite of repeated careful $F \rightarrow F_H$ conversion experiments). Phenomenologically we can describe these behaviors with rather shallow unsymmetric $U(z^*)$ potential as depicted in Fig. 7: for RbCl:OH^- basically without any potential well for B and only a shallow one for R with an U_R state, from which thermally activated transitions into close lying states above the small energy barrier occur already at very low temperatures. For KCl, the $U(z^*)$ potential does not show any distinct minima with localized U_R and U_B states, allowing rapid reorientational motion of the OH^- and a wide linear z vibration of the K_γ^+ already at lowest temperatures. The EA(T) behavior of these two systems should also be quite different from the bistable ones, as discussed above: In RbCl, the EA_R absorption existent at 4 K should become totally exchanged into EA_{HT} already at 20 K, while in KCl the total observed EA band could consist only of EA_{HT} absorption over the whole range of temperature. Similar as in the bistable systems, the observed EA_{HT} for both RbCl and KCl lie again on the low-energy side of the F band again indicating a K_γ^+ (or $Rb)_\gamma^+$ shift away from the F electron. This ''high-temperature phase'' behavior is in fact supported by ENDOR measurements in KCl:OH^-, in which (opposite to the case of KBr:OH^-) the response could be followed up to high temperatures. This study yielded a z motion of K_γ^+ of large amplitude (which increases with temperature) and a time-averaged K_γ^+ displacement away from the F center.

We left out so far any discussion of two important VA results, observed in all bistable systems:

(a) The two VA_R and VA_B lines (both about equally sharp at 4 K), show in all cases under temperature increase a much stronger *spectral broadening* for R compared to the B line (as clearly seen in Fig. 4 for one example of KBr:OH^-). We interpret this in terms of our $U(z^*)$ model by very different coupling and sensitivity of the OH^- oscillator to the K_γ^+ motion along the z axis [see Fig. 7(a)]. For the R configuration this z motion lies parallel to the OH^- orientation and can by its time-varying repulsive interaction along the axis of the OH^- strongly modify its oscillator frequency and/or force it into a large amplitude coupled librational motion away from the z axis. In contrast to this, in the B configuration the OH^- is oriented perpendicular to (and rotates rapidly around) the z axis, such that its oscillator frequency is much less affected and coupled to the vibrational z motion of the K_γ^+ ion.

(b) Similarly interesting is the result (obtained from Δ VA measurements like in Figs. 1–3, that the *oscillator strength* is considerably (2–3.5 times) higher for the VA_R compared to the VA_B (see Table I). This is much more difficult to interpret for several reasons: Even for the isolated OH^-, the transition dipole moment dp/dr is negative[29] (due to redistribution of the electronic density under vibration), is highly nonlinear due to strong ''electric anharmonicity,'' and changes in its strength $(dp/dr)^2$ considerably under host and isotope variation.[30] Moreover, the transition probability should be quite sensitive to the electronic environment and its polarizability. We have in fact observed for CN^- defects that the proximity of a highly polarizable electronic defect (e.g., F center) can strongly enhance the effective $(dp/dr)^2$ value.[31] A full interpretation of the observed f_R/f_B result, we still leave open as a challenging unanswered question.

Basically all our reported VA measurements and their treatment with the $U(z^*)$ model potential were dealing with the F center in its $1s$ ground state. The only exception from this is the optical $B \rightleftarrows R$ conversion at 4 K which we used as a convenient experimental tool to change the B:R ratio from its thermal equilibrium and subsequently study its recovery towards this value (see Fig. 5). As we observed a very high (0.2–0.6) quantum efficiency for the optical conversion processes (see Fig. 6 and Table II), it is worth to briefly discuss and try to explain this in the framework of our model. After the Born-Oppenheimer $1s \rightarrow 2p$ transition of a pure F center, all equivalent surrounding ions (particularly the six NN cations . . .) are no longer in thermal equilibrium and relax rapidly ($\sim$ps) towards new positions in the lattice. For our $F_H(OH^-)$ center essentially the same will occur for its five ''normal NN cation neighbors,'' but something very different for its special NN K_γ^+ neighbor initially located at the z_R or z_B minima of a very shallow two-well $U(z^*)_{1s}$ potential. The drastic change of electronic distribution and polarizability by the $1s \rightarrow 2p$ transition will bring this shallow potential out of its thermal equilibrium, thus inducing an extremely rapid z^* motion of the coupled K_γ^+ and OH^- ions towards the minimum of a very different new $U(z^*)_{2p}$ potential. Without predicting anything about the shape (or new minimum) of this potential, we only conclude that during the rapid first electron-lattice relaxation process the positions of K_γ^+ and OH^- strongly change, inducing of course also reorientation of the OH^-. After relaxation of the F electron and return to the $U(z^*)_{1s}$ potential, the system will be left in a unrelaxed state away from the thermal equilibrium in terms of its K_γ^+ and OH^- position and orientation. From this state (which most likely lies above the potential barrier) the system can ultimately relax with similar probability into either the R or B potential well. In order to explain the ''fractional'' quantum efficiency we have to assume that during the excitation/relaxation cycle the system ''loses memory'' about the B or R configuration from which it originated. Furthermore, the system must relax (or ''cool down'') in the recovered $U(z^*)_{1s}$ potential extremely rapidly, avoiding any ''thermalization'' between the B and R state occupations; otherwise a nonthermal equilibrium could not be achieved by the optical cycling process.

In the following papers II and III, in which all experiments are performed under intense optical pumping, much more details about E-V energy transfer and time dependence of the optical cycle will be measured and discussed. As one important input from this paper I, the determined high quantum efficiency of $B \rightleftarrows R$ conversions will play an important role in the interpretations, particularly of the kinetics of the optical excitation/relaxation cycle.

ACKNOWLEDGMENT

Support of this work by NSF Grant No. DMR-92-23230 is gratefully acknowledged.

[1] See, e.g., W. B. Fowler, in *Physics of Color Centers* (Academic, New York, 1968), Chap. 2.
[2] See, e.g., W. Gellermann, J. Phys. Chem. Solids **52**, 249 (1991).
[3] D. Pan and F. Luty, Phys. Rev. B **18**, 1868 (1978).
[4] M. Leblans, W. Joosen, D. Schoemaker, A. Mabud, and F. Luty, Phys. Rev. B **39**, 8657 (1989).
[5] Y. Yang and F. Luty, Phys. Rev. Lett. **51**, 419 (1983).
[6] L. Gomez and F. Luty, Phys. Rev. B **30**, 7194 (1984).
[7] Y. Yang and F. Luty, J. Lumin. **40**, 565 (1988).
[8] W. Gellermann, Y. Yang, and F. Luty, Opt. Commun. **57**, 196 (1986).
[9] F. Rong, Y. Yang, and F. Luty, Cryst. Latt. Defects Amorph. Mater. **18**, 1 (1989).
[10] C. E. Mungan, U. Happek, and A. J. Sievevs, J. Lumin. **58** (1–6), 33 (1994).
[11] M. Krantz and F. Luty, Phys. Rev. B **37**, 8412 (1988).
[12] G. Halama, K. T. Tsen, S. H. Liu, F. Luty, and J. B. Page, Phys. Rev. B **39**, 13 457 (1989).
[13] L. Gomez and F. Luty, Phys. Rev. B **52**, 7094 (1995).
[14] S. Kapphan and F. Luty, J. Phys. Chem. Solids **34**, 969 (1973).
[15] S. Söthe, J. M. Spaeth, and F. Luty, J. Phys. Condens. Matter **5**, 1957 (1993).
[16] G. Baldacchini, S. Botti, U. M. Grassano, L. Gomez, and F. Luty, Europhys. Lett. **9**, 735 (1989).
[17] E. Gustin, M. Leblans, A. Bouwen, D. Schoemaker, and F. Luty, following paper, Phys. Rev. B **54**, 6963 (1996).
[18] E. Gustin, M. Leblans, A. Bouwen, D. Schoemaker, and F. Luty, this issue, Phys. Rev. B **54**, 6977 (1996).
[19] A. Afanasiev and F. Luty, Solid State Commun. **98**, 531 (1996).
[20] It should be noted that the $B \rightarrow R$ conversions performed for the VA measurements are often incomplete and can differ from one measurement to another due to the high optical density in the electronic absorption of the thick samples which are favorable to see the VA. This does, however, not influence the following observed trends.
[21] G. Baldacchini, in *Nonlinear Spectroscopy of Solids*, edited by B. Di Bartolo, NATO ASI Series (Plenum, New York, 1994), p. 339.
[22] L. Bosi and M. Nimis, Nuovo Cimento **13**, 377 (1991).
[23] S. Okazaki, N. Ohtori, and I. Okada, J. Chem. Phys. **92**, 7505 (1990).
[24] F. J. Adrian, A. N. Jette, and J. M. Spaeth, Phys. Rev. B **31**, 3923 (1985).
[25] H. F. Ivey, Phys. Rev. **72**, 341 (1947).
[26] H. Härtel, Phys. Status Solidi **42**, 369 (1970).
[27] G. K. Pandey and D. K. Shukla, Phys. Rev. B **4**, 4598 (1985).
[28] S. Kapphan, J. Phys. Chem. Solids **35**, 621 (1974).
[29] H. J. Werner, P. Rasmus, and E.-A. Reinsch, J. Chem. Phys. **79**, 905 (1983).
[30] A. Afanasiev, C. P. An, and F. Luty, *Defects in Insulating Materials* (World Scientific, Singapore, 1994), p. 551.
[31] V. Dierolf and F. Luty, *Defects in Insulating Materials* (Ref. 30), p. 17.